Defining Lagrangian coherent vortices from their trajectories

Anass El Aouni, Khalid Daoudi, Hussein Yahia, Suman Kumar Maji, Khalid Minaoui

Defining Lagrangian coherent vortices from their trajectories

A. El Aouni,[1, a)] K. Daoudi,[1] H. Yahia,[1] S. Maji,[2] and K. Minaoui[3]
[1)]*Geostat team, INRIA Bordeaux Sud-Ouest, Talence, France*
[2)]*Indian Institute of Technology Patna, India*
[3)]*University Mohammed V in Rabat, LRIT, Morocco*

(Dated: 20 December 2019)

We study the transport properties of mesoscale eddies (i.e. vortices of $100 \sim 200$ km in diameter) over a finite time duration. While these oceanic structures are well-known to stir and mix surrounding water, they can also carry and transport water properties in a coherent manner. In this paper, we are interested in dynamic transport properties of these coherent structures, despite their chaotic environment. Here, we reveal that such vortices can be identified based a simple decomposition of their Lagrangian trajectories. We identify and extract coherent vortices as material lines along which particles' trajectories share similar polar rotations. The proposed method identifies coherent vortices and their centers in automatic manner. We illustrate our new method by identifying and extracting Lagrangian coherent vortices in different two-dimensional flows.

I. INTRODUCTION

Lagrangian coherent structures (LCSs) are exceptional material surfaces that shape finite-time observed tracer patterns in fluid flows[1]. In the geophysical fluid dynamics community, these LCSs are mainly structured into three physical shapes; mesoscale and submesoscale filaments, jets and eddies. These latter oceanic structures are ubiquitous in the ocean and usually exhibit different properties to their surrounding waters. They are known to stir and mix surroundings fluid as well as by their ability to trap and carry fluid properties in a coherent manner. For example, long-lived eddies such as Agulhas eddies are known to transport water properties associated with the Indian ocean far into the South Atlantic[2]. In this work, we focus on those that remain coherent despite the chaotic nature of their environment. These mesoscale eddies are also known by their important role in climate change, which arises from their influence on the circulation by transporting temperature and salinity, extracting potential energy from the mean flow and exchanging momentum with it. They are also known to help maintaining the extra-tropical climate by contributing to the meridional transport of heat from the tropics to the poles[3].

As the effect of these mesoscale eddies on the global circulation is remarkable, their systematic and accurate detection has received considerable interest over the last two decades[4–7]. In the literature, several definitions of vortices have been introduced together with their automatic detection[8–11], most of these formulations are of Eulerian nature. For instance, authors in[12] proposed a vorticity curvature criterion method to identify coherent vortices. An ω_R criterion for vortex identification has been proposed in[13], their method works by measuring the relative rotation strength on the plane perpendicular to the local rotation axis. Authors in[14] defines a vortex as a connected flow region where the magnitude of the vortex vector at each point is larger than zero. Such Eulerian approaches make use of instantaneous velocity field to detect vortices boundaries which fail to coherently carry and transport their encircled water masses, instead, they stretch, deform and develop filaments. For example, the angular velocity $\omega = \frac{d\phi}{dt}$ is considered as an Eulerian approach to identify vortices' boundaries. Fig.1(a) shows eddies' boundaries extracted from the angular velocity computed over the southern ocean. Fig.1(b) (Multimedia view) shows their final position after three months of Lagrangian advection. None of these eddies remains coherent, indeed they all stretch and filament. Their complete advection sequence is illustrated in the movie M1 (Multimedia view).

On the other hand, Lagrangian methods are powerful tools because they take into account the time-evolution of particles' trajectories[6,7,15,16]. Various methods have been proposed within this perspective, they typically fall into different classes: probabilistic, which study the evolution of probability densities and almost-invariant sets[5,17,18], and geometric which use invariant manifolds. Authors in[6] introduce a variational principle for coherent material vortices, where vortices' boundaries are sought as elliptic LCSs, i.e. exceptional material barriers that exhibit no appreciable stretching or folding over a finite time interval. This method has been reformulated such that it can be solved via the variational level set methodology[19]. Another method has been proposed which seeks vortices' boundaries as maximal material tubes in which material elements complete the same polar rotation over a given finite-time interval[20]. However, these stretching-based variational methods rely on a precise computation of Cauchy-green tensor and its invariants, which requires accurate differentiation of particles trajectories with respect to their initial positions. Authors in[7] proposed a vorticity-based method to identify rotational coherent vortices. This has been done based on a decomposition of gradient deformation into product of two deformation gradients; one for pure strain and other for pure rotation[21]. This approach does not require differentiation of the flow map with respect to initial conditions. However, it relies on derivatives of the velocity field, and requires a large computational domain for spatial mean of vorticity. Authors in[22] adapted the latter technique to use it on magnetic fields and proposed a method of integrated averaged current deviation to determine the boundary of magnetic vortices. Authors in[23] used the spectral clustering algorithm to identify coherent structures by grouping Lagrangian particles into coherent and incoherent. This has been done by defining coher-

[a)]Electronic mail: anas.elaouni@gmail.com

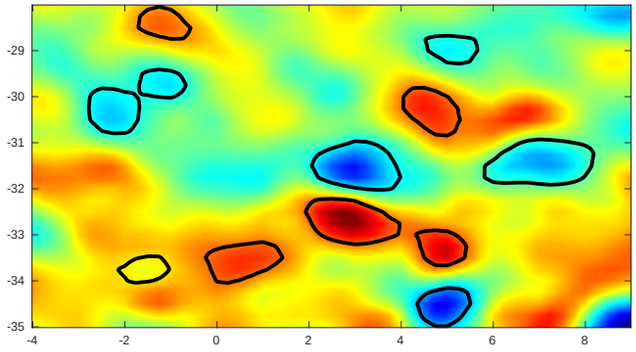

(a)

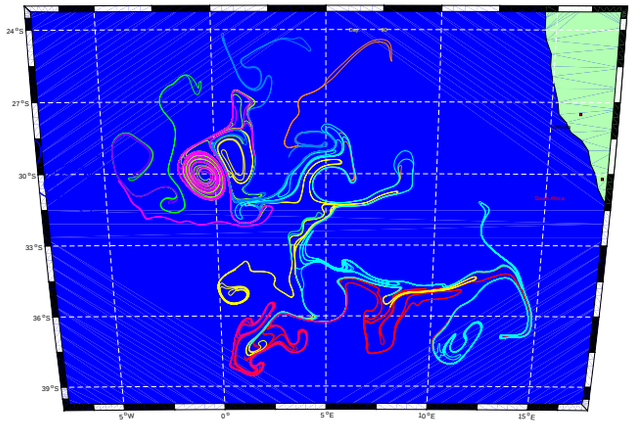

(b)

FIG. 1: a) Eulerian eddies defined as outermost contours of the angular velocity's extrema. b) Their final positions under Lagrangian advection over three months. (See the supplemental movie M1 (Multimedia view) for the complete advection sequence of these eddies' boundaries).

ent structures as a set of Lagrangian trajectories that maintain short distances among themselves relative to the others outside the structure. This method is simple to implement but has no link between material vortices and the expected spinning motion. On the other hand, authors in[15] defined Lagrangian vortices from their observed trajectories, their method indeed has a link between material vortices and the expected spinning motion. They defined Lagrangian coherent vortices from their frequency-domain representation, they defined them as closed material surfaces along which particles share similar frequency components. Their method is simple to implement and suitable to applications to float data because it does not rely on velocity field.

The approach proposed in the present paper is based on a decomposition of particle trajectory into two parts: closed curves which give information about uniformly rotating flow, and the second part which describes the mean displacement. The former part yields a consistent measure of material rotation. In this work, we seek to identify Lagrangian coherent vortex boundary as closed material lines in which fluid parcels complete the same polar rotation, therefore a Lagrangian vortex is defined as an evolving domain enclosed by this latter. This turns out to be filled with outward-increasing closed contours of the Averaged Closed Curve ($\mathscr{ACC}$). Additionally, $\mathscr{ACC}-$based vortex's center is defined as the innermost member of $\mathscr{ACC}$. Our method is based on vortices trajectories, and it has several important features:

- It is naturally related to vortex feature and defines vortices based on their observed trajectories.
- Material $\mathscr{ACC}$-vortices guarantee the revolving movement of all particles within vortices' boundaries. At least, all particles rotate 360° around the observed center.
- Our method does not require differentiation of flow map with respect to initial conditions.
- The images produced by $\mathscr{ACC}$ map itself gives insight into the qualitative evolution of different particles' trajectories.
- It is suitable to applications to float data.
- $\mathscr{ACC}$ is generic, it can be adapted with the finite-size notion. The method can be set up to be more selective, where it can require particles' trajectories to complete a certain number of closed curves. Thus, it could lump vortices with different lifetimes into the same scalar field.

This paper is organized as follows: Section II describes the setup and outlines the main computational tool. Section III discusses and illustrates particles trajectories in vortex boundary. Section IV presents, details our new approach. Section V illustrate our method via different fluid simulations. Conclusion is drawn in the last Section.

II. SET-UP

We consider a time-dependent smooth vector field:

$$\mathbf{v}(\mathbf{x},t), \quad \mathbf{x}\in\mathbb{R}^2, \quad t\in[\alpha,\beta] \tag{1}$$

and its associated ordinary differential equation:

$$\dot{\mathbf{x}} = \mathbf{v}(\mathbf{x},t), \quad \mathbf{x}\in\mathbb{R}^2, \quad t\in[\alpha,\beta] \tag{2}$$

where $\mathbf{v}$ a smooth velocity field defined on a possibly time-dependent spatial domain $\mathbf{U}(t)\subset\mathbb{R}^2\times[\alpha,\beta]$.

The flow map is defined as the map that takes a particle from its initial location $\mathbf{x}_0$ at time t_0 to its location $\mathbf{x}_t$ at time t:

$$\mathbf{F}_{t_0}^{t}(\mathbf{x}_0) := \mathbf{x}(t,t_0,\mathbf{x}_0), \quad \alpha\le t_0\le t\le\beta, \tag{3}$$

$\mathbf{x}(t,t_0,\mathbf{x}_0)$ denoting the trajectory of Eq.2 passing through a point $\mathbf{x}_0$ at time t_0.

Consider a material line $\mathscr{M}(t_0)$ advected by the flow. Its image at time t can be expressed in term of the flow map as $\mathscr{M}(t) = \mathbf{F}_{t_0}^{t}(\mathscr{M}(t_0))$.

We write the trajectory's arc-length of a given particle $\mathbf{x}_0$ traveling in the flow between the time interval $[t_0, t_f]$ as:

$$\mathscr{L}(\mathbf{x}(t_f,t_0,\mathbf{x}_0)) = \int_{t_0}^{t_f} \|\mathbf{v}(\mathbf{x}_0,t)\|\,dt \tag{4}$$

The arc-length of this trajectory can be approximated in term of flow map as:

$$\mathscr{L}(\mathbf{x}(t_f,t_0,\mathbf{x}_0)) = \sum_{i=1}^{f} \left\| \mathbf{F}_{t_0}^{t_i}(\mathbf{x}_0) - \mathbf{F}_{t_0}^{t_{i-1}}(\mathbf{x}_0) \right\| \tag{5}$$

With $\left\| (\mathbf{F}_{t_0}^{t_i}(\mathbf{x}_0) - \mathbf{F}_{t_0}^{t_{i-1}}(\mathbf{x}_0)) \right\|$ a line segment of a given particle $\mathbf{x}_0$ traveling between the time interval $[t_{i-1}, t_i]$.

III. PARTICLES TRAJECTORY IN VORTEX BOUNDARY

Particle trajectory produced by integrating the velocity vector field in a vortex boundary result into a loopy curve which intersects itself (Fig.2(a,b,c)). Thus, a possible way to identify Lagrangian coherent vortices is by computing the number of closed curves in given particles' trajectories. That is the number n of times when a given particle $\mathbf{x}$'s trajectory crosses itself at $t_i+\tau_i$, $\mathbf{x}(t_i+\tau_i) = \mathbf{x}(t_i)$ and creates a closed curve such as:

$$\mathbf{x}(t_i+\tau_i) = \mathbf{x}(t_i), \quad \tau_i > 0 \quad \text{with} \quad i = 1 \cdots n \quad (a)$$

$$t_i \in]t_0\ t_f[, \quad t_{i+1} \notin [t_i\ t_i+\tau_i[\quad (b) \tag{6}$$

and

$$\mathbf{x}(t_{i+1}) \notin]\mathbf{x}(t_i)\ \mathbf{x}(t_i+\tau_i)[\quad (c)$$

Where τ_i is the period of time for a particle starting at t_i takes to cross its trajectory, whereas t_{i+1} refers to the time position of the next closed-curve $\mathbf{x}(t_{i+1}+\tau_{i+1}) = \mathbf{x}(t_{i+1})$. Here, (a) defines a closed curve, whereas, (b) and (c) insure that the next intersection at t_{i+1} is not within the previous closed-curve $\mathbf{x}(t_i+\tau_i) = \mathbf{x}(t_i)$. Fig.2 displays 3 different scenarios of particles initialized in vortices boundaries, closed curves satisfying conditions in eq.6 are highlighted in red color.

Computing the number of closed curves for all particles might give an idea about the location of potential vortices. Such idea might identify vortices as homogeneous regions where particles' trajectories have similar number of closed-curve (vortices where particles have similar angular velocity), or the number of closed curves increases toward their centers and decreases in inverse proportion to the distance from the centers (vortices where the angular velocity increases toward their centers). However, this picture won't give a precise location of vortices boundaries due to the fact particles' trajectories within a vortex boundary might not have the same number

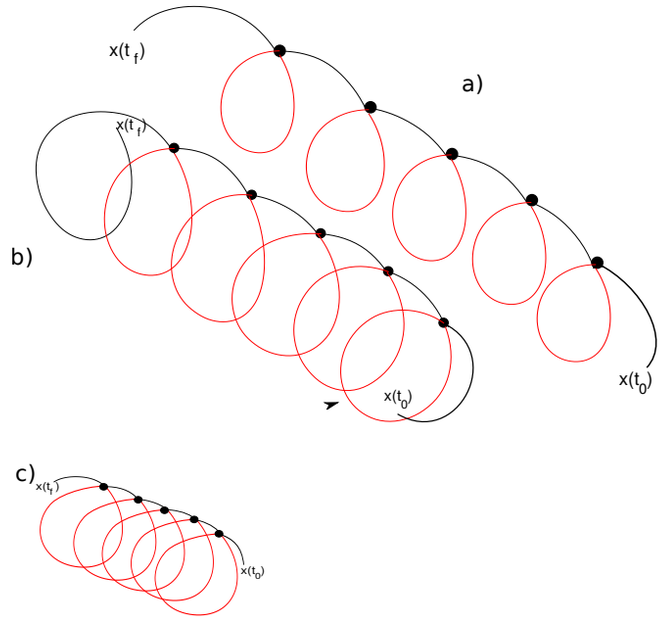

FIG. 2: a,b and c) 3 particles' trajectories with different angular velocities; closed curves satisfying eq.6 are highlighted in red color.

of closed curves due to their initial location and finite-time advection. Fig.3(a) shows two trajectories of two particles within the same vortex boundary advected for the same time interval $[t_0\ t_f]$; one exhibits 5 closed curves while the other has 6 closed curves. On the other hand, Fig.3(b) shows this idea applied on velocity field derived from satellite altimetry over the southern ocean, where region of high spinning are highlighted.

IV. DEFINING VORTEX BOUNDARY FROM PARTICLES TRAJECTORY

In this part, we aim to define Lagrangian coherent vortices from their trajectories. We seek to identify these structures as closed material lines along which particles exhibit similar rotations around the same axis, and over the same finite time interval. We have seen in the previous section that particles within the same vortex boundary can have similar trajectories but not necessarily the same number of closed curves. In this work, we choose to decompose Lagrangian trajectories into two parts; closed curves which give information about uniformly rotating flow, and the second part that describes the mean displacement. Here, we only consider the former part which is most closely related to the nature of vortices.

We define the Averaged Closed Curve metric ($\mathscr{ACC}$) as:

$$\mathscr{ACC}(\mathbf{x}(t_f,t_0,\mathbf{x}_0)) = \sum_{i=1}^{n} \frac{\int_{t_i}^{t_i+\tau_i} \|\mathbf{v}(\mathbf{x}_0,t)\|\,dt}{n} \tag{7}$$

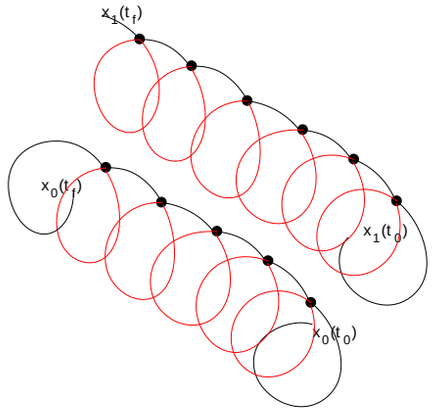

(a)

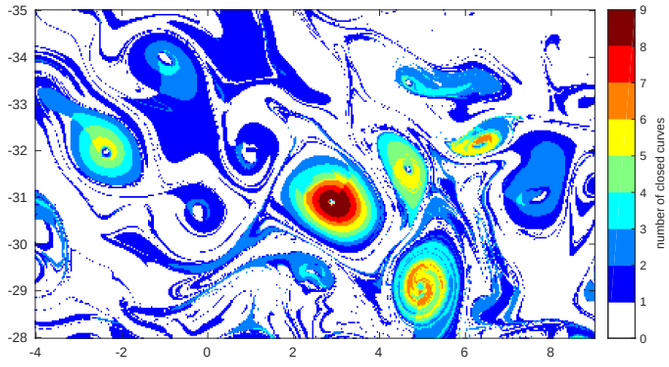

(b)

FIG. 3: a) Trajectory of two particles within the same vortex's boundary and advected for the same period of time; both have different number of closed curves. b) Regions of potential vortices: number of closed curves computed from sea surface velocity field derived from satellite altimetry over the southern ocean.

such as

$$\mathbf{x}(t_i+\tau_i)=\mathbf{x}(t_i),\quad \tau_i>0 \quad \text{with} \quad i=1\cdots n$$
$$,$$
$$t_i\in]t_0\ t_f[,\quad t_{i+1}\notin[t_i\ t_i+\tau_i[\qquad (8)$$
$$\text{and}$$
$$\mathbf{x}(t_{i+1})\notin]\mathbf{x}(t_i)\ \mathbf{x}(t_i+\tau_i)[$$

With n being the number of segments of a given particle $\mathbf{x}$ trajectory satisfying eq.8. Where τ_i is the period of time for a particle initialized at t_i to return to the same point at $t_i+\tau_i$. Fig.4(a) shows an example of a particle trajectory and its segments satisfying the eq.8. On the other hand, Fig.4(b) shows the geometric view of the $\mathscr{ACC}$ approach. In similar way, we show the geometric view of the $\mathscr{ACC}$ method applied on a particle trajectory within a vortex with a radial flow where all particles converge toward its attracting center in Fig.5. For a fluid parcel starting from $\mathbf{x}_0$, the $\mathscr{ACC}^t_{t_0}(\mathbf{x}_0)$ field is dynamically consistent measure material rotation.

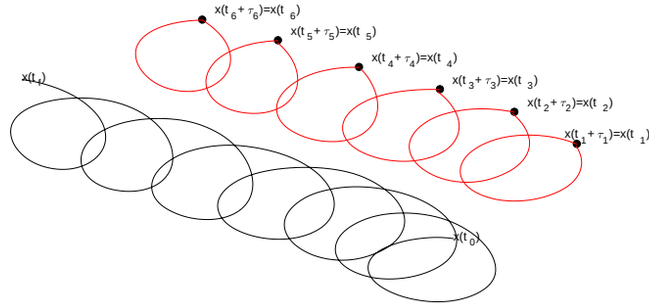

(a)

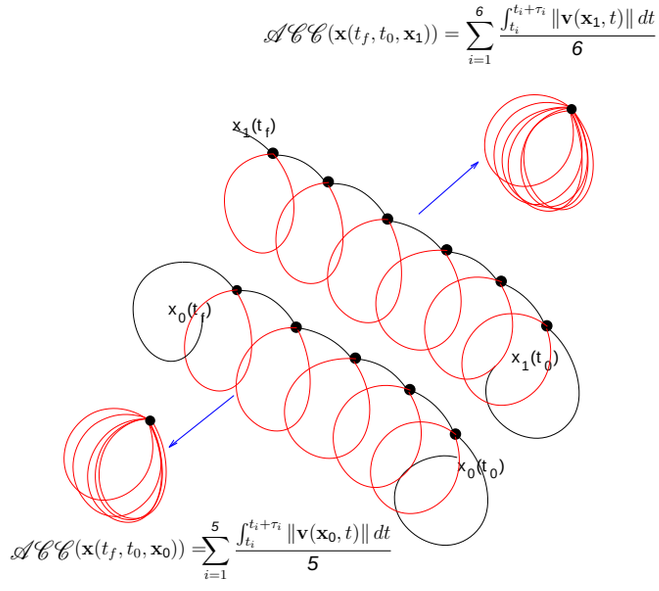

(b)

FIG. 4: a) (black) Trajectory of particle within vortex boundary, (red) segments satisfying equation 8. b) Example of $\mathscr{ACC}^{t_f}_{t_0}$ calculation of two partilcles within the same vortex's boundary.

We now use the $\mathscr{ACC}$ to identify vortex boundary as material line along which fluid parcels experience the same polar rotation over the same time interval $[t_0,t_f]$. Time t_0 positions of such material lines are contours of the function $\mathscr{ACC}^{t_f}_{t_0}$. The inner-most member of such nested sequences of contours, with inward decreasing $\mathscr{ACC}$ values, defines the vortex center. In similar way, the outer-most contour defines the vortex's boundary. At least, all particles within the vortex boundary have to complete one polar rotation to allow their identifi-

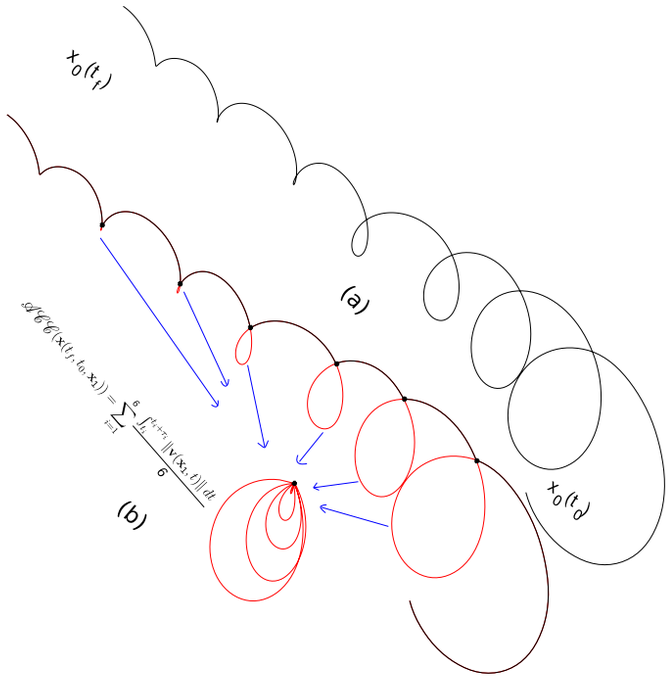

FIG. 5: (black) Trajectory of particle within a vortex with a radial flow where particles converge toward its center, (red) segments satisfying equation 8. b) Example of $\mathscr{ACC}_{t_0}^{t_f}$ calculation of this converging trajectory.

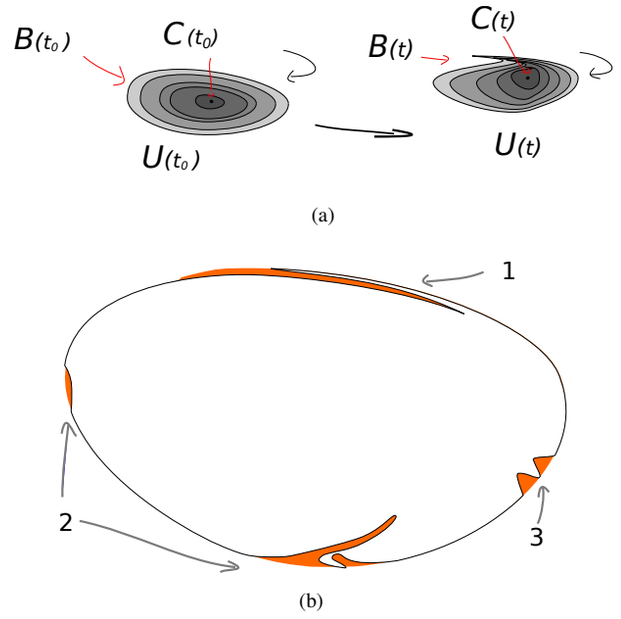

FIG. 6: a) Initial and time t positions of a Lagrangian coherent vortex $\mathbf{U}(t)$, its boundary $\mathbf{B}(t)$ and center $\mathbf{C}(t)$. b) An example of a closed material line which profits from the relaxation of convexity to small convexity deficiency. Orange area indicates the area difference between the closed material line and its convex hull: (1) minor tangential filamentation, (2) deformation by smaller-scale vortices, (3) discrete approximation of a convexity.

cation. We summarize the $\mathscr{ACC}$-based vortex identification approach in the following definition, with its geometry illustrated in Fig.6(a):

Definition 1 *for a given time interval* $[t_0,t_f]$*:*

- *1) Lagrangian coherent vortex is an evolving material domain* $\mathbf{U}(t) \subset \mathbb{R}^2 \times [t_0,t_f]$ *such that* $\mathbf{U}(t_0) \subset \mathbb{R}^2$ *is filled with a nested family of contours of* $\mathscr{ACC}_{t_0}^{t_f}(\mathbf{x}_0)$ *with outward-increasing* $\mathscr{ACC}$ *values.*
- *2) The boundary* $\mathbf{B}(t) \subset \mathbb{R}^2 \times [t_0,t_f]$ *of* $\mathbf{U}(t)$ *is the outermost convex contours of* $\mathscr{ACC}_{t_0}^{t_f}(\mathbf{x}_0)$ *in* $\mathbf{U}(t_0)$*.*
- *3) The center* $\mathbf{C}(t) \subset \mathbb{R} \times [t_0,t_f]$ *of* $\mathbf{U}(t)$ *is defined as the innermost (minimum) member of* $\mathscr{ACC}_{t_0}^{t_f}(\mathbf{x}_0)$ *in* $\mathbf{U}(t_0)$*.*

In the computational world, we relax the convexity strictness for closed material surface of $\mathscr{ACC}$. The first reason for this convexity relaxation consists of allowing small tangential filamentation even at time t_0 of vortices' boundaries (Fig.6-b-1). The second reason consists of the nature of multi-scale data, such data shows the presence of small-scale vortices nearby the boundaries of big-scale vortices (Fig.6-b-2). The third reason consists of the representation of vortices' boundaries by discrete polygons (Fig.6-b-3). At the initial time t_0, the definition 1 identify Lagrangian coherent vortices with a simple geometry, that is by defining a parameter of maximal convexity deficiency d_{max} to allow the relaxation of convexity strictness. This enables capturing filamented parts that rotate together with the vortices without a global breakaway. The aforementioned definition allows the identification of vortex boundary $\mathbf{B}(\mathbf{t_0})$ which has convexity deficiency less than the maximal limit d_{max}. We define the convexity deficiency of a closed curve in the plane as the ratio of the area difference between the curve and its convex hull to the area enclosed by the curve as: $d = \frac{A(Conv(\mathbf{B}(\mathbf{t_0})))-A(\mathbf{B}(\mathbf{t_0}))}{A(\mathbf{B}(\mathbf{t_0}))}$. Fig.6-b shows the geometrical view of the convexity deficiency parameter, the orange color refers to the difference between the curve (in white) and its convex hull.

Lagrangian vortices, as well as their boundaries and centers, are materials objects[7,15,24]. Thus, their position at a given time t is only determined by Lagrangian advection:

$$\begin{aligned} \mathbf{U}(t) = \mathbf{F}_{t_0}^{t}(\mathbf{U}(t_0)), \quad \mathbf{B}(t) = \mathbf{F}_{t_0}^{t}(\mathbf{B}(t_0)) \\ \mathbf{C}(t) = \mathbf{F}_{t_0}^{t}(\mathbf{C}(t_0)), \quad t \in [t_0,t_f] \end{aligned} \tag{9}$$

The $\mathscr{ACC}$-vortex approach differs from the previous definitions, it does define vortex based on its observed trajectory, more precisely closed-curves segments of its particles' trajectories. As no differentiation of particles trajectories with respect to their initial positions is required, our approach does not require advection of high-density grids. $\mathscr{ACC}$-vortex may show material filament, but by definition, these filamented parts will rotate together with the vortex without breaking away. An interesting feature of our approach is its

ability to include the notion of finite-size by requiring particles' trajectory to complete a certain number closed-curves. In this case, the present method could lump vortices occurring over different time intervals into the same scalar field. This could be interesting in geophysical flows applications.

V. EXPERIMENTS

This section presents numerical results that confirm our theoretical predictions regarding the identification of coherent vortices.

A. Direct numerical simulation of two-dimensional turbulence

We solve numerically the Navier-Stokes PDE model for the time evolution of 2 components of the velocity, $u : \mathscr{D} \to \mathbb{R}^2$ of an incompressible fluid on a torus, $\mathscr{D} = [0, 2\pi] \times [0, 2\pi]$. This can be expressed as:

$$\begin{aligned} \partial u_t + u \cdot \nabla u &= -\nabla p + \frac{1}{Re}\Delta u + f, && (x,t) \in \mathscr{D} \times [a,b], \\ \nabla \cdot u &= 0, && (x,t) \in \mathscr{D} \times [a,b], \\ \int u^j dx &= 0, && (x,t) \in \mathscr{D} \times [a,b], j = 1,2, \\ u &= u^*, && (x,t) \in \mathscr{D} \times \{0\} \end{aligned} \tag{10}$$

Where $u \cdot \nabla u$ is the inertial term which characterizes Navier-Stokes equation, and is responsible for the transfer of kinetic energy in the turbulent cascade. ∇p is the pressure gradients which guarantee the incompressibility of the flow, and $\frac{1}{Re}\Delta u$ is the the dissipative viscous term. We further assume periodic boundary conditions and use a standard pseudo-spectral method with 512 modes in each direction and $2/3$ dealiasing to solve the above Navier-Stokes equation with Reynolds number $Re = 10^4$ on the time interval $t \in [0, 1600]$. The model is parameterized by the pressure function $p : D \times [a,b] \to \mathbb{R}$, with no external forcing ($f = 0$). We initialize the system with the vorticity of two adjacent vortices perturbed by a random uniform distribution:

$$\begin{aligned} \overline{\omega}|_{t_0} = exp(&\frac{(x-\pi)^2 + (y-2\pi-\pi/4)^2}{0.2}) \\ &- exp(\frac{(x-\pi-\pi/4)^2 + (y-\pi-\pi/4)^2}{0.8}) \end{aligned} \tag{11}$$

We use the vorticity stream formulation[25] for implementation and get back velocity and pressure from the stream function. The flow integration is then carried out over a uniform grid of 512×512 and over the interval $t \in [400, 1600]$, in which the turbulent flow is under fully developed turbulence, by a fourth-order Runge-Kutta method with variable step-size.

Fig.8(a) shows coherent vortices and their centers extracted from the $\mathscr{ACC}^{I_f}_{t_0}(\mathbf{x}_0)$ map applied on the simulated realization of fluid velocity of the model 10. Fig. 8(b) (Multimedia view) shows their final position under Lagrangian advection as well as trajectories of their centers. These vortices remain coherent, their boundaries do not stretch or ford. The complete advection sequence over the time interval [0, 1200] is illustrated in the movie M2 (Multimedia view).

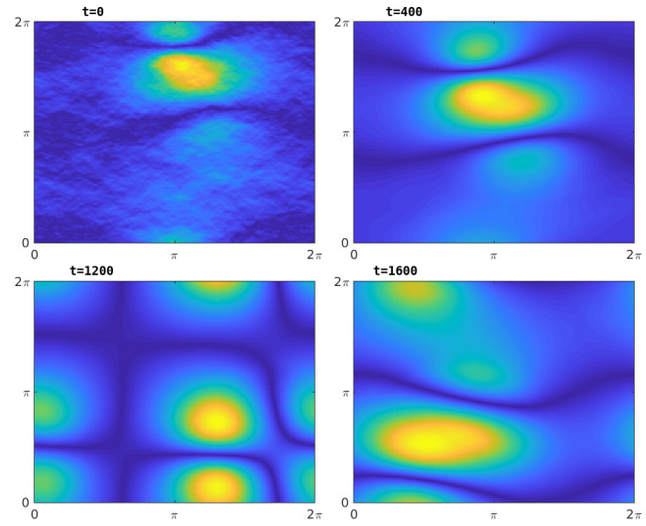

FIG. 7: Time evolution of the magnitude of fluid velocity governed by the Navier–Stokes model 10, over two spatial dimensions: the angle of the inner ring (horizontal axis) and outer ring (vertical axis) of a two-dimensional torus. Angles are expressed in radians. Velocity field is evaluated at times $t = (0,\ 400,\ 1200,\ 1600)$.

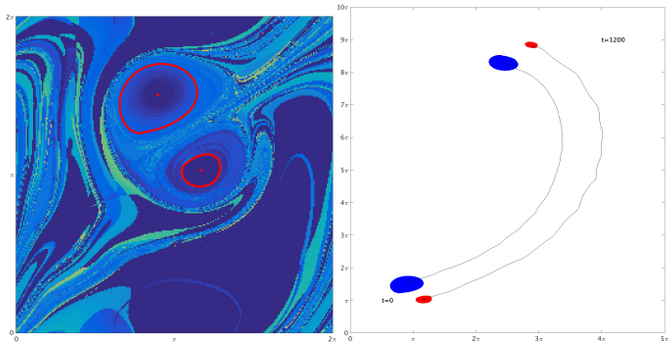

(a) (b)

FIG. 8: a) Coherent vortices and their centers at time t_0 extracted from the velocity field generated by Navier–Stokes model 2 using definition.1 with the $\mathscr{ACC}^{I_f}_{t_0}(\mathbf{x}_0)$ map shown in background. b) Their initial and final positions under Lagrangian advection. (See the supplemental movie M2 (Multimedia view) for the complete advection sequence of these vortices).

B. Two-dimensional eddies in satellite altimetry

Here, we use sea surface velocity data to illustrate the detection of Lagrangian vortices. This velocity data is derived from satellite altimetry under the geostrophic approximation where sea-surface height $\eta(\varphi,\theta,t)$ serves as a non-canonical Hamiltonian for surface velocities in the (φ,θ) longitude-latitude coordinate system. The evolution of fluid particles satisfies:

$$\begin{aligned}\dot{\varphi}(\varphi,\theta,t) &= -\frac{g}{R^2 f(\theta)\cos\theta}\partial_\theta \eta(\varphi,\theta,t)\\ \dot{\theta}(\varphi,\theta,t) &= \frac{g}{R^2 f(\theta)\cos\theta}\partial_\varphi \eta(\varphi,\theta,t)\end{aligned} \tag{12}$$

where g is the constant of gravity, R is the mean radius of the Earth and $f(\theta)=2\Omega\sin\theta$ is the Coriolis effect, with Ω denoting the Earth's mean angular velocity. This data is produced by Ssalto/duacs multi-mission sea level products provided by AVISO (CLS/Archiving, Validation, and Interpretation of Satellite Oceanographic data)[26] with a spatial resolution of $1/4^\circ$ and temporal resolution of 7 days. We chose the region of the Agulhas leakage in the Southern Ocean, spans from $[-28^\circ N,-4^\circ W]$ and $[-35^\circ N,9^\circ W]$. This region is well known for its long-lived propagating eddies that carry water properties from the Indian ocean far into the South Atlantic[2]. In this study, we chose the time period between 11/11/2006 and 11/1/2007. We integrate the AVISO dataset (eq.12) over the period of time between $t_0=11$ November 2006 and $t_f=t_0+90$ days over an initial grid of particles with step size $\Delta x_0=1/50^\circ$.

We show in Fig.9(a) the $\mathscr{ACC}_{t_0}^{t_f}(\mathbf{x}_0)$ map computed from the satellite velocity field (eq.12). At the same image, we show eddies' boundaries and their centers extracted from the $\mathscr{ACC}$ map. In Fig.9(b) (Multimedia view), we show their initial and final position under Lagrangian advection as well as trajectories of their centers. These eddies remain coherent, their boundaries do not stretch or fold. The complete advection sequence over the time interval [0, 90] is illustrated in the movie M3 (Multimedia view).

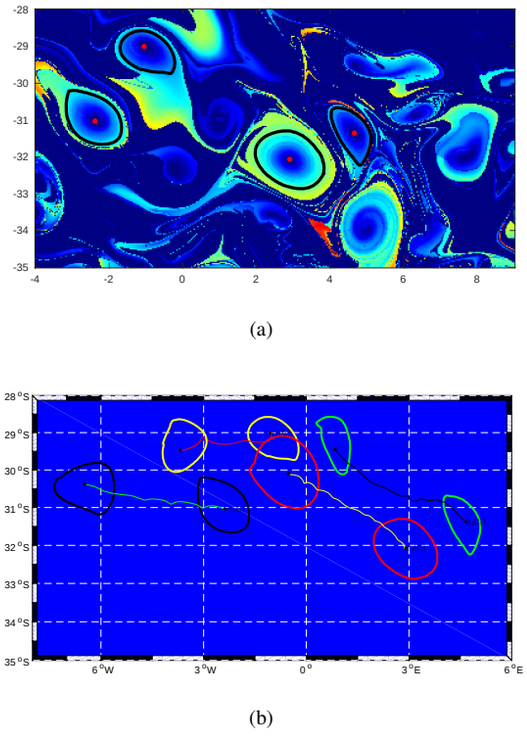

(a)

(b)

FIG. 9: a) Coherent eddies and their centers at time t_0 extracted using definition.1 with the $\mathscr{ACC}_{t_0}^{t_f}(\mathbf{x}_0)$ map shown in background. b) Their initial and final positions under Lagrangian advection. (See the supplemental movie M3 (Multimedia view) for the complete advection sequence of these vortices.)

VI. INERTIAL PARTICLES IN GEOSTROPHIC LAGRANGIAN VORTEX

Here, we illustrate our method over a vortex with a radial flow where particles converge toward its attracting center. Consider a small spherical particle of radius r_0 and density ρ_{part} in a geostrophic flow of density ρ and viscosity ν. Here we consider the β-plane approximation. By applying a slow-manifold reduction to the Maxey-Riley equations[27] in the limit of small Rossby numbers, it has been shown by[28] that the inertial particle motion satisfies:

$$\dot{\mathbf{x}}=\mathbf{v}(\mathbf{x},t)+\tau(\delta-1)f\mathbf{J}\mathbf{v}(\mathbf{x},t)+\mathscr{O}(\tau^2),\quad \mathbf{J}=\begin{pmatrix}0&-1\\1&0\end{pmatrix},\quad \mathbf{x}\in\mathbb{R}^2,\quad t\in[\alpha,\beta] \tag{13}$$

with f being the Coriolis parameter, and:

$$\delta=\frac{\rho}{\rho_{part}},\quad \tau:=\frac{2r_0^2}{9\nu\delta}, \tag{14}$$

Remarkably, in the limit of vanishing Rossby numbers, cyclones attract light particles ($\delta>1$) and anticyclones attract heavy particles ($\delta<1$) in (eq.13). We select the computational domain between $[2^\circ W,4^\circ W]$ and $[-30^\circ N,-32^\circ N]$, which falls inside the region of the Agulhas leakage in the Southern Ocean.

We consider the AVISO dataset covering the period between $t_0=11$ November 2006 and $t_f=t_0+90$ days. We integrate this satellite velocity data (12) using the Maxey-Riley equation (eq.13). Inertial particles were assumed to have $r_0=0.25m$, which is a realistic radius for commonly used spherical drifting buoys. Both light and heavy particles were considered, with $\delta=1.1$ and 0.9 respectively. We show in Fig.10(a) an example of this eddy and its center extracted from the $\mathscr{ACC}_{t_0}^{t_f}(\mathbf{x}_0)$ map. Fig.10(b) (Multimedia view) shows its initial and final positions under Lagrangian advection, also in the same image Lagrangian trajectories of two heavy particles released in different positions within the eddy. This confirms that eddy's boundary does not fold or filament under Lagrangian advection even when it shrinks by time. This also

shows that the $\mathscr{ACC}$-based vortex centers act as attractors for heavy particles released in anticyclones. The complete advection sequence over the time interval $[0, 90]$ is illustrated in the movie M4 (Multimedia view).

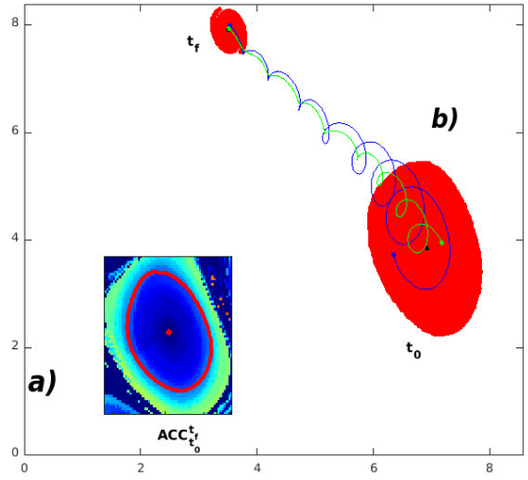

FIG. 10: a) Coherent anticyclone and its center at time t_0 extracted using definition.1 with the $\mathscr{ACC}_{t_0}^{t_f}(\mathbf{x}_0)$ map shown in background. b) Its initial and final positions under Lagrangian advection. At the same image, trajectories of two heavy particles released inside the anticyclone. (See the supplemental movie M4 (Multimedia view) for the complete advection sequence of this anticyclone).

VII. CONCLUSION

The present paper defines Lagrangian vortices from their observed trajectory. It defines these vortices as closed material lines in which fluid parcels exhibit similar rotation. These latter are obtained based on particle trajectory decomposition. In this work, coherent vortices boundaries are expressed as convex contours of the Averaged Closed Curve ($\mathscr{ACC}$) map. On the other hand, their centers are extracted as the most-inner member of $\mathscr{ACC}$. The proposed approach is illustrated on different two-dimensional fluid flows. Results show that vortices boundaries and their centers obtained are sharply defined, do not fold or filament. The proposed method has the advantage of not requiring high-grids advection of fluid parcels. It is suitable to applications to float data. Moreover, it can be adapted to select votrices boundaries occurring over different time interval.

ACKNOWLEDGMENTS

A. El Aouni was supported by the PHC project n° TBK/16-24 and the French Project BOOSTE TON DOC 2019.

[1]T. Peacock and G. Haller, "Lagrangian coherent structures: The hidden skeleton of fluid flows," Physics today **66**, 41 (2013).
[2]W. d. Ruijter, A. Biastoch, S. Drijfhout, J. Lutjeharms, R. Matano, T. Pichevin, P. v. Leeuwen, and W. Weijer, "Indian-atlantic interocean exchange: Dynamics, estimation and impact," Journal of Geophysical Research: Oceans **104**, 20885–20910 (1999).
[3]R. Farneti, T. L. Delworth, A. J. Rosati, S. M. Griffies, and F. Zeng, "The role of mesoscale eddies in the rectification of the southern ocean response to climate change," Journal of Physical Oceanography **40**, 1539–1557 (2010).
[4]D. Karrasch, F. Huhn, and G. Haller, "Automated detection of coherent lagrangian vortices in two-dimensional unsteady flows," in *Proc. R. Soc. A*, Vol. 471 (The Royal Society, 2015) p. 20140639.
[5]G. Froyland, N. Santitissadeekorn, and A. Monahan, "Transport in time-dependent dynamical systems: Finite-time coherent sets," Chaos: An Interdisciplinary Journal of Nonlinear Science **20**, 043116 (2010).
[6]G. Haller and F. Beron-Vera, "Coherent lagrangian vortices: The black holes of turbulence," Journal of Fluid Mechanics **731** (2013).
[7]G. Haller, A. Hadjighasem, M. Farazmand, and F. Huhn, "Defining coherent vortices objectively from the vorticity," Journal of Fluid Mechanics **795**, 136–173 (2016).
[8]L. Zhang, Q. Deng, R. Machiraju, A. Rangarajan, D. Thompson, D. K. Walters, and H.-W. Shen, "Boosting techniques for physics-based vortex detection," in *Computer Graphics Forum*, Vol. 33 (Wiley Online Library, 2014) pp. 282–293.
[9]J. Sahner, T. Weinkauf, N. Teuber, and H.-C. Hege, "Vortex and strain skeletons in eulerian and lagrangian frames," IEEE Transactions on Visualization and Computer Graphics **13** (2007).
[10]M. Herrmann, "A eulerian level set/vortex sheet method for two-phase interface dynamics," Journal of Computational Physics **203**, 539–571 (2005).
[11]M. Serra and G. Haller, "Objective eulerian coherent structures," Chaos: An Interdisciplinary Journal of Nonlinear Science **26**, 053110 (2016).
[12]J. Elsas and L. Moriconi, "Vortex identification from local properties of the vorticity field," Physics of Fluids **29**, 015101 (2017).
[13]X. Dong, Y. Gao, and C. Liu, "New normalized rortex/vortex identification method," Physics of Fluids **31**, 011701 (2019).
[14]C. Liu, Y. Gao, S. Tian, and X. Dong, "Rortex—a new vortex vector definition and vorticity tensor and vector decompositions," Physics of Fluids **30**, 035103 (2018).
[15]A. El Aouni, H. Yahia, K. Daoudi, and K. Minaoui, "A fourier approach to lagrangian vortex detection," Chaos: An Interdisciplinary Journal of Nonlinear Science **29**, 093106 (2019).
[16]G. Haller, "An objective definition of a vortex," Journal of fluid mechanics **525**, 1–26 (2005).
[17]G. Froyland, "An analytic framework for identifying finite-time coherent sets in time-dependent dynamical systems," Physica D: Nonlinear Phenomena **250**, 1–19 (2013).
[18]G. Froyland, C. Horenkamp, V. Rossi, N. Santitissadeekorn, and A. S. Gupta, "Three-dimensional characterization and tracking of an agulhas ring," Ocean Modelling **52**, 69–75 (2012).
[19]A. Hadjighasem and G. Haller, "Level set formulation of two-dimensional lagrangian vortex detection methods," Chaos: An Interdisciplinary Journal of Nonlinear Science **26**, 103102 (2016).
[20]M. Farazmand and G. Haller, "Polar rotation angle identifies elliptic islands in unsteady dynamical systems," Physica D: Nonlinear Phenomena **315**, 1–12 (2016).
[21]G. Haller, "Dynamic rotation and stretch tensors from a dynamic polar decomposition," Journal of the Mechanics and Physics of Solids **86**, 70–93 (2016).
[22]E. Rempel, A.-L. Chian, F. J. Beron-Vera, S. Szanyi, and G. Haller, "Objective vortex detection in an astrophysical dynamo," Monthly Notices of the Royal Astronomical Society: Letters **466**, L108–L112 (2016).
[23]A. Hadjighasem, D. Karrasch, H. Teramoto, and G. Haller, "Spectral-clustering approach to lagrangian vortex detection," Physical Review E **93**, 063107 (2016).
[24]G. Haller, "Lagrangian coherent structures," Annual Review of Fluid Mechanics **47**, 137–162 (2015).
[25]W. Spotz, *High-order compact finite difference schemes for computational mechanics*, Ph.D. thesis, University of Texas at Austin Austin, TX (1995).
[26]Http://www.aviso.oceanobs.com/duacs/.
[27]M. R. Maxey and J. J. Riley, "Equation of motion for a small rigid sphere in a nonuniform flow," The Physics of Fluids **26**, 883–889 (1983).

[28]F. J. Beron-Vera, M. J. Olascoaga, G. Haller, M. Farazmand, J. Triñanes, and Y. Wang, "Dissipative inertial transport patterns near coherent lagrangian eddies in the ocean," Chaos: An Interdisciplinary Journal of Nonlinear Science **25**, 087412 (2015).

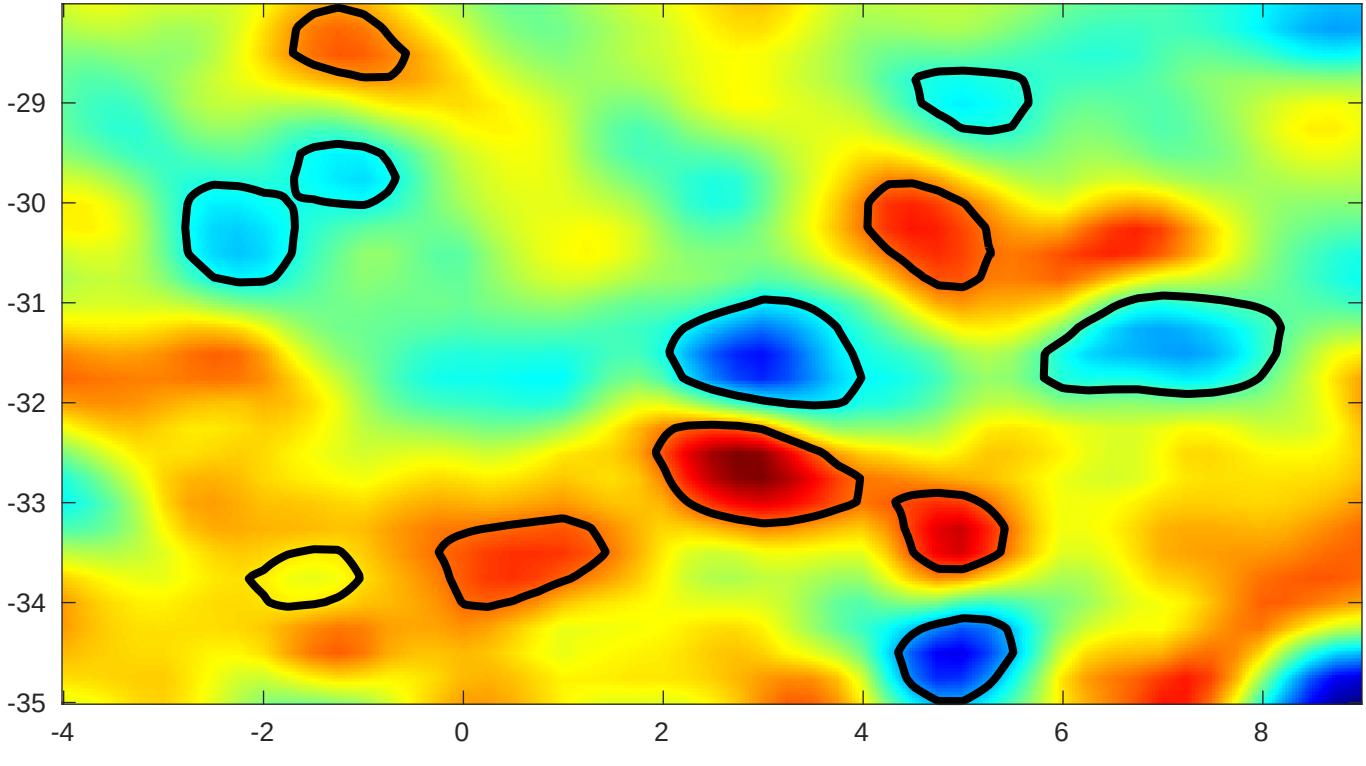
-29
-30
-31
-32
-33
-34
-35
-4
-2
0
2
4
6
8

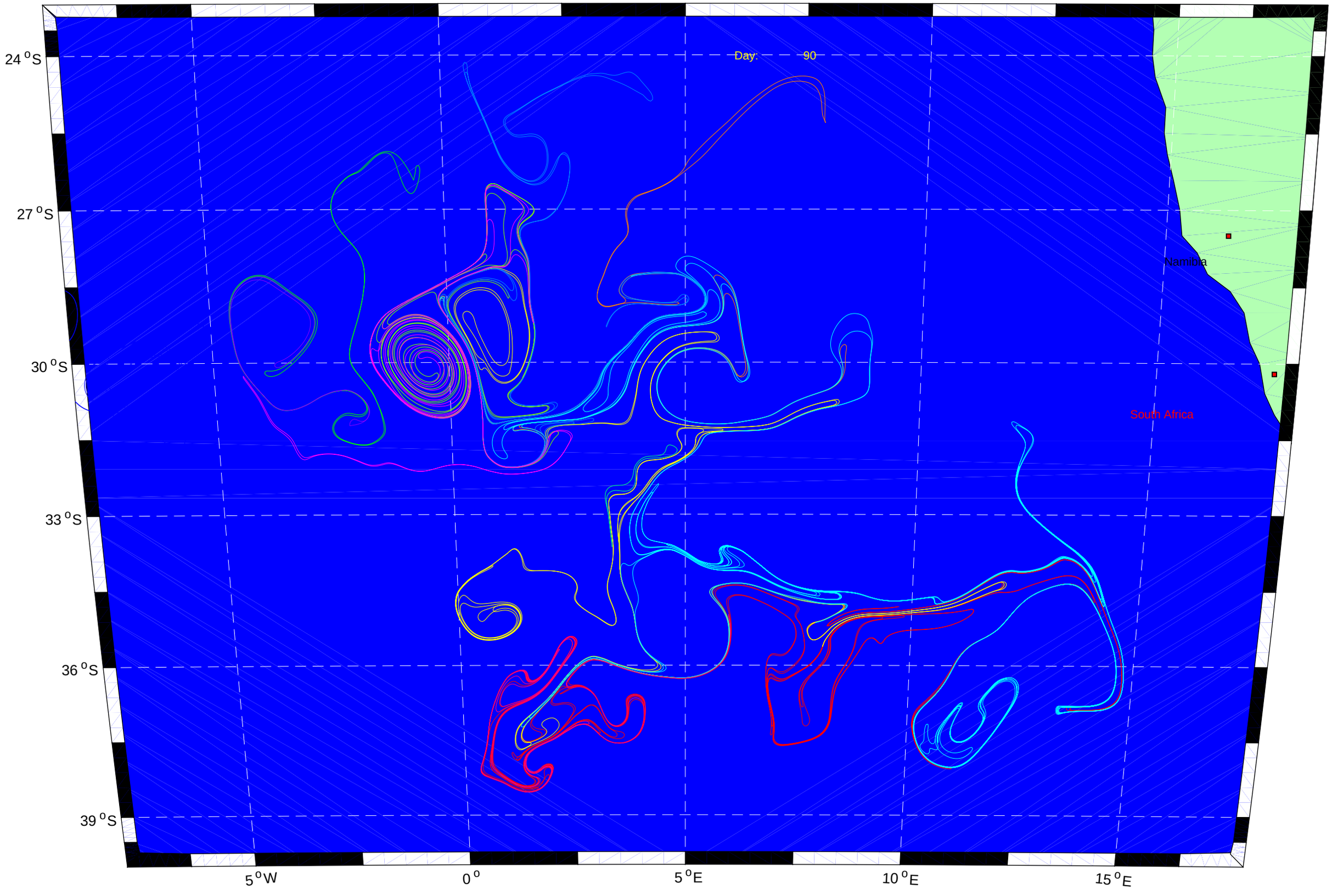
Day: 90
Namibia
South Africa
24 °S
27 °S
30 °S
33 °S
36 °S
39 °S
5 °W
0 °
5 °E
10 °E
15 °E

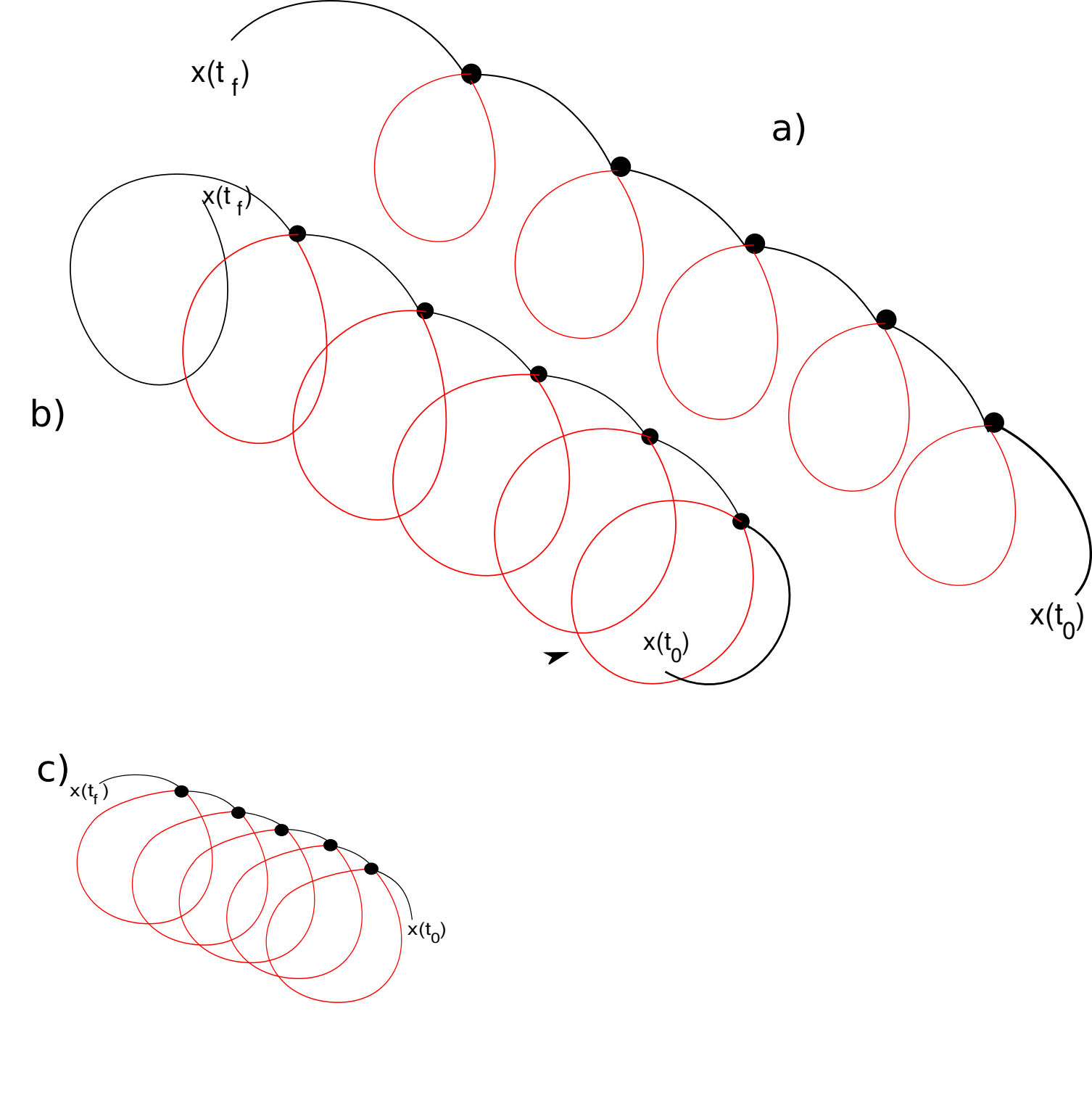
x(t f)
a)
x(t f)
b)
x(t0)
x(t0)
c)
x(tf)
x(t0)

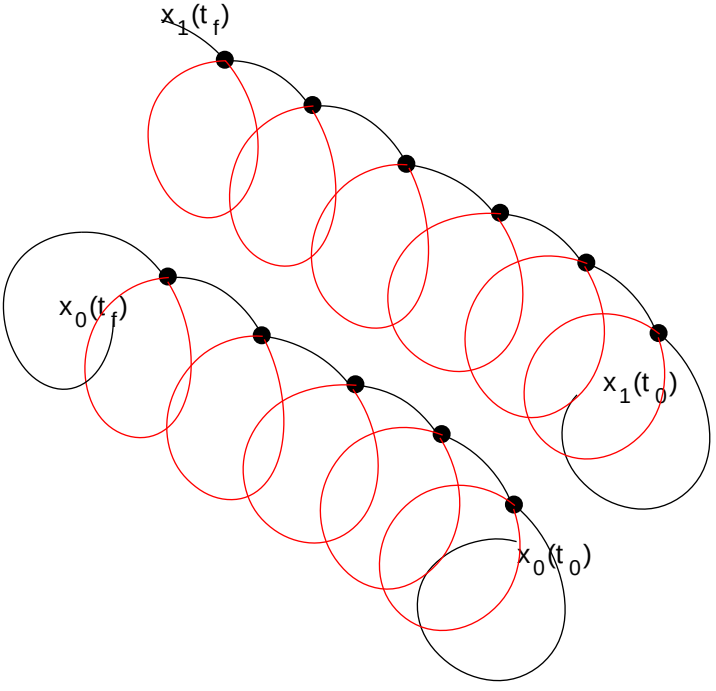
$x_1(t_f)$
$x_0(t_f)$
$x_1(t_0)$
$x_0(t_0)$

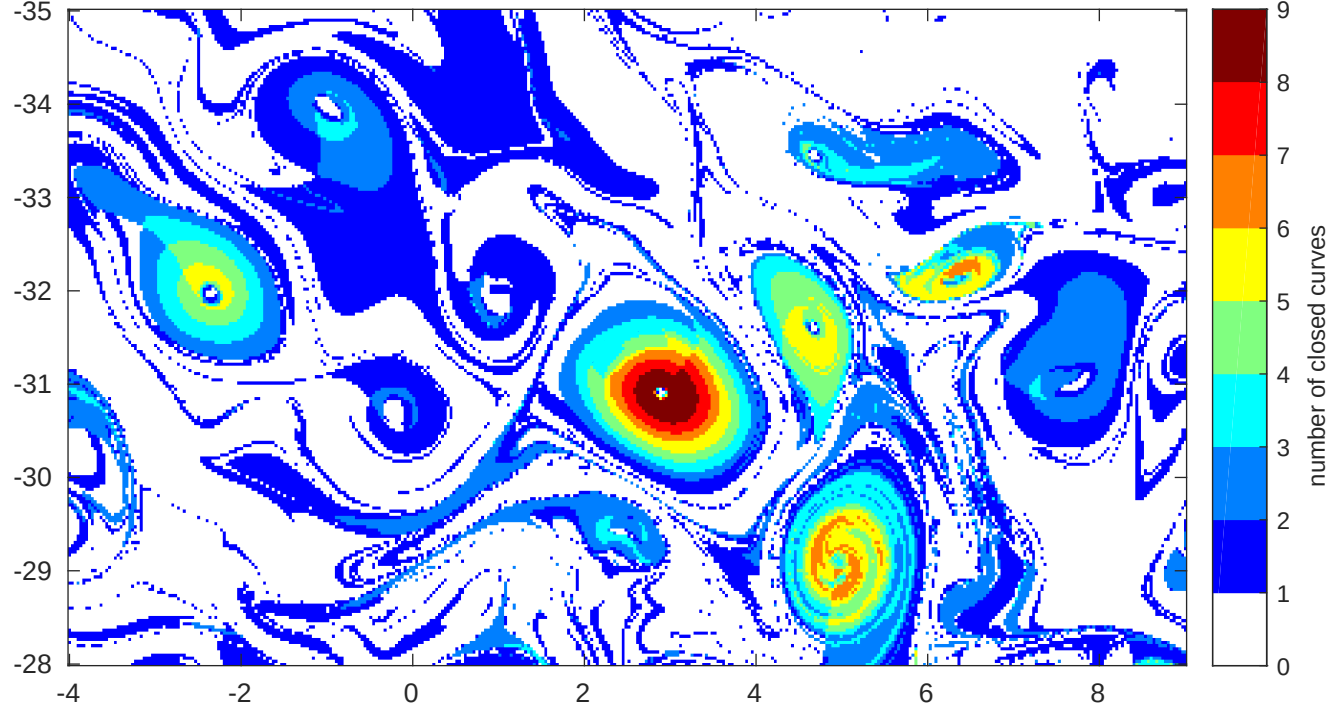
-35
-34
-33
-32
-31
-30
-29
-28
-4
-2
0
2
4
6
8
9
8
7
6
5
4
3
2
1
0
number of closed curves

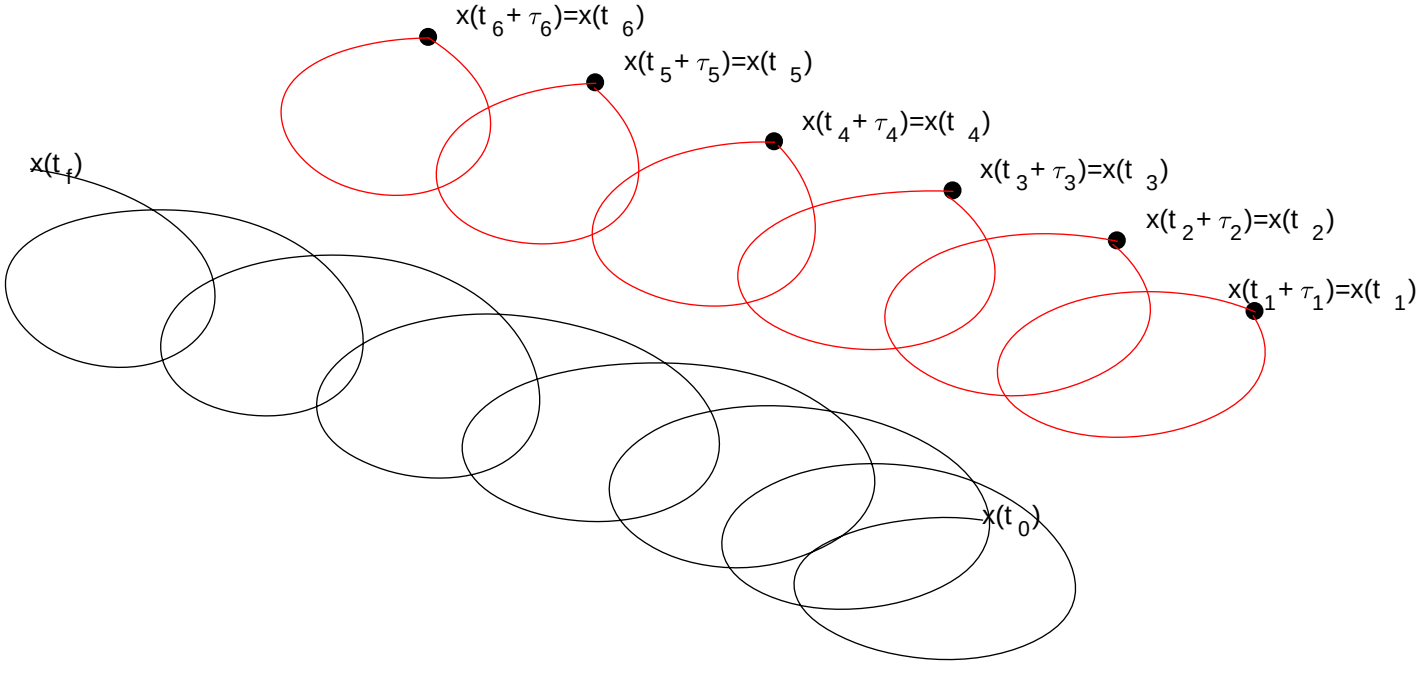
x(t 6 + τ6)=x(t 6)
x(t 5 + τ5)=x(t 5)
x(t 4 + τ4)=x(t 4)
x(t 3 + τ3)=x(t 3)
x(t 2 + τ2)=x(t 2)
x(t 1 + τ1)=x(t 1)
x(t f)
x(t 0)

$$\mathscr{ACC}(\mathbf{x}(t_f, t_0, \mathbf{x}_1)) = \sum_{i=1}^{6} \frac{\int_{t_i}^{t_i+\tau_i} \|\mathbf{v}(\mathbf{x}_1, t)\|\, dt}{6}$$

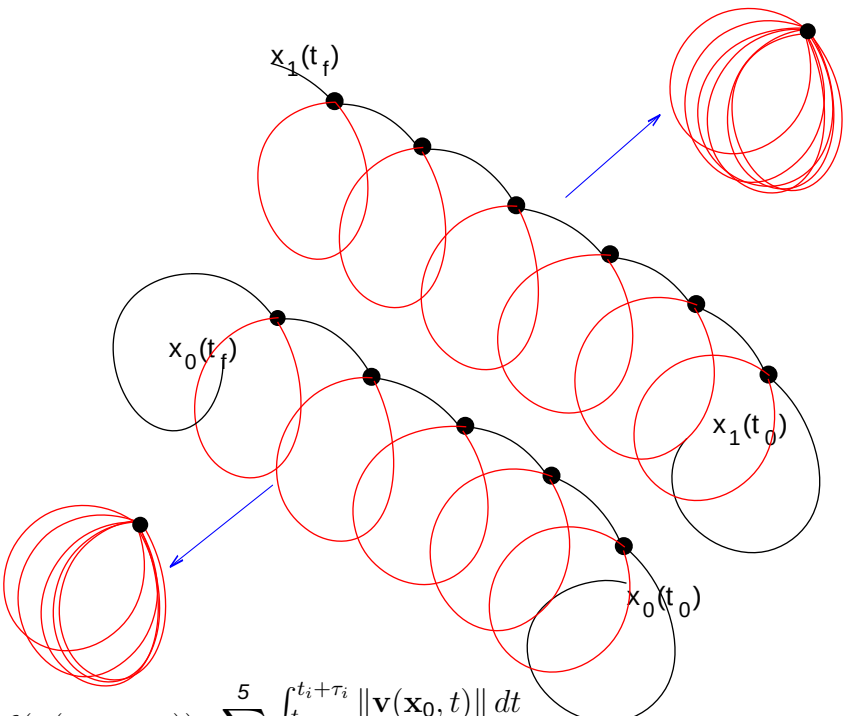

$$\mathscr{ACC}(\mathbf{x}(t_f, t_0, \mathbf{x}_0)) = \sum_{i=1}^{5} \frac{\int_{t_i}^{t_i+\tau_i} \|\mathbf{v}(\mathbf{x}_0, t)\|\, dt}{5}$$

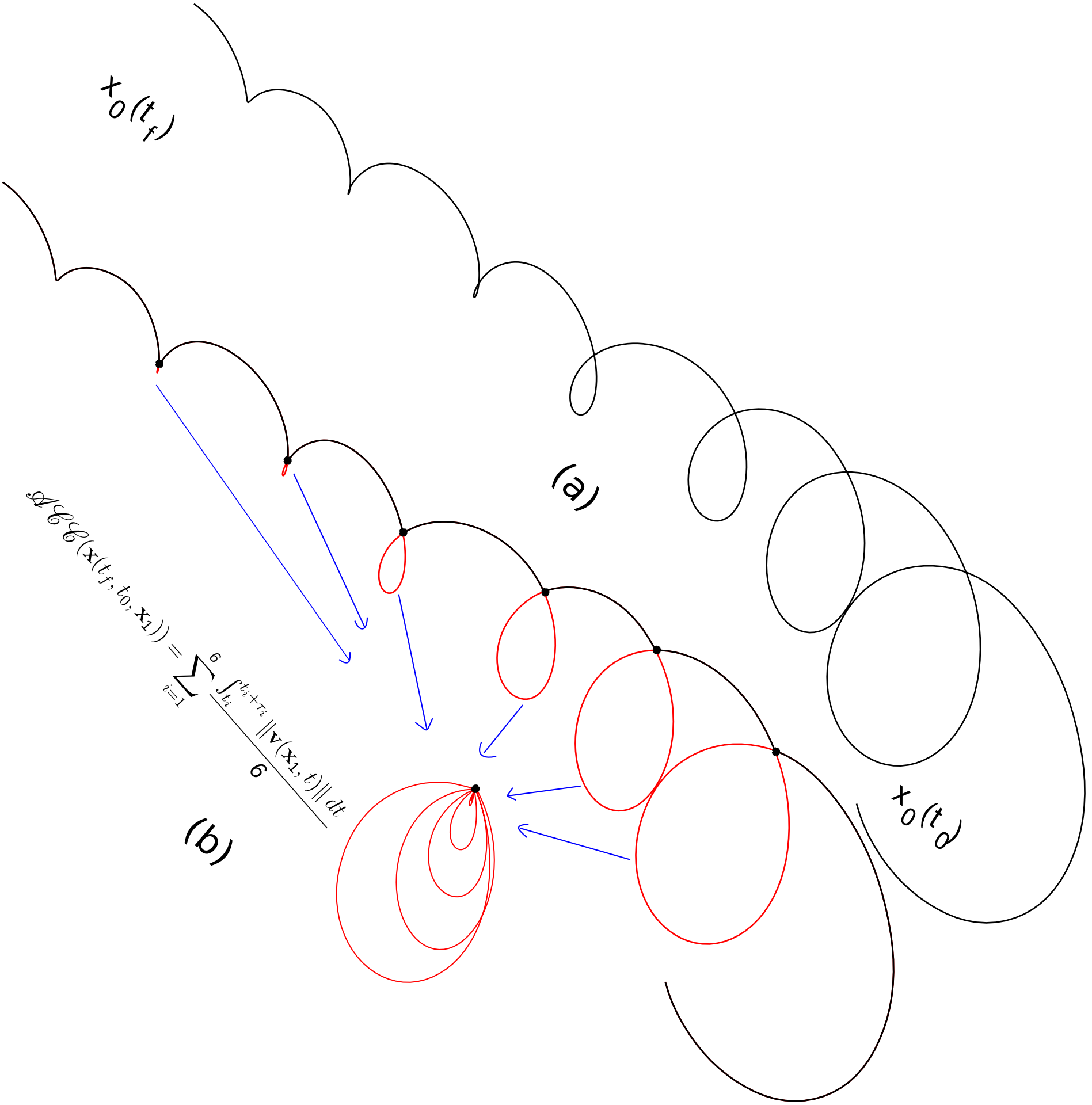
$x_0(t_f)$
(a)
$\mathscr{AGB}(\mathbf{x}(t_f, t_0, \mathbf{x}_1)) = \sum_{i=1}^{6} \frac{\int_{t_i}^{t_i+\tau_i} \|\mathbf{v}(\mathbf{x}_1, t)\| \, dt}{6}$
(b)
$x_0(t_0)$

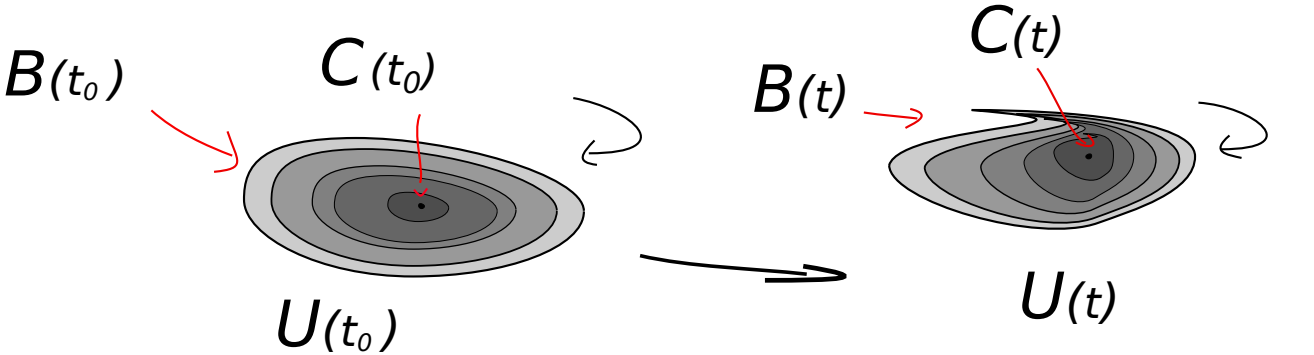
$B_{(t_0)}$
$C_{(t_0)}$
$U_{(t_0)}$
$B_{(t)}$
$C_{(t)}$
$U_{(t)}$

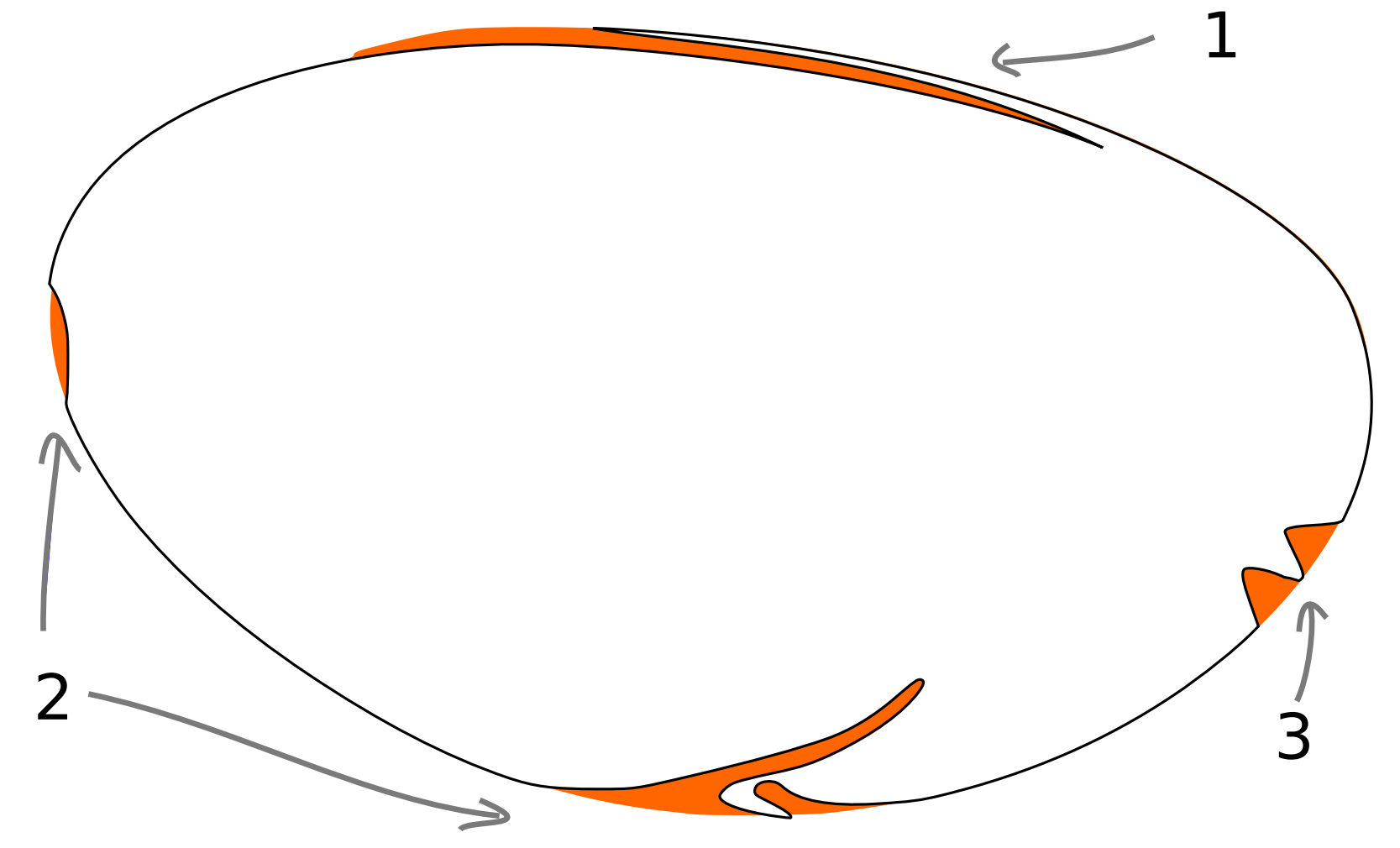
1
2
3

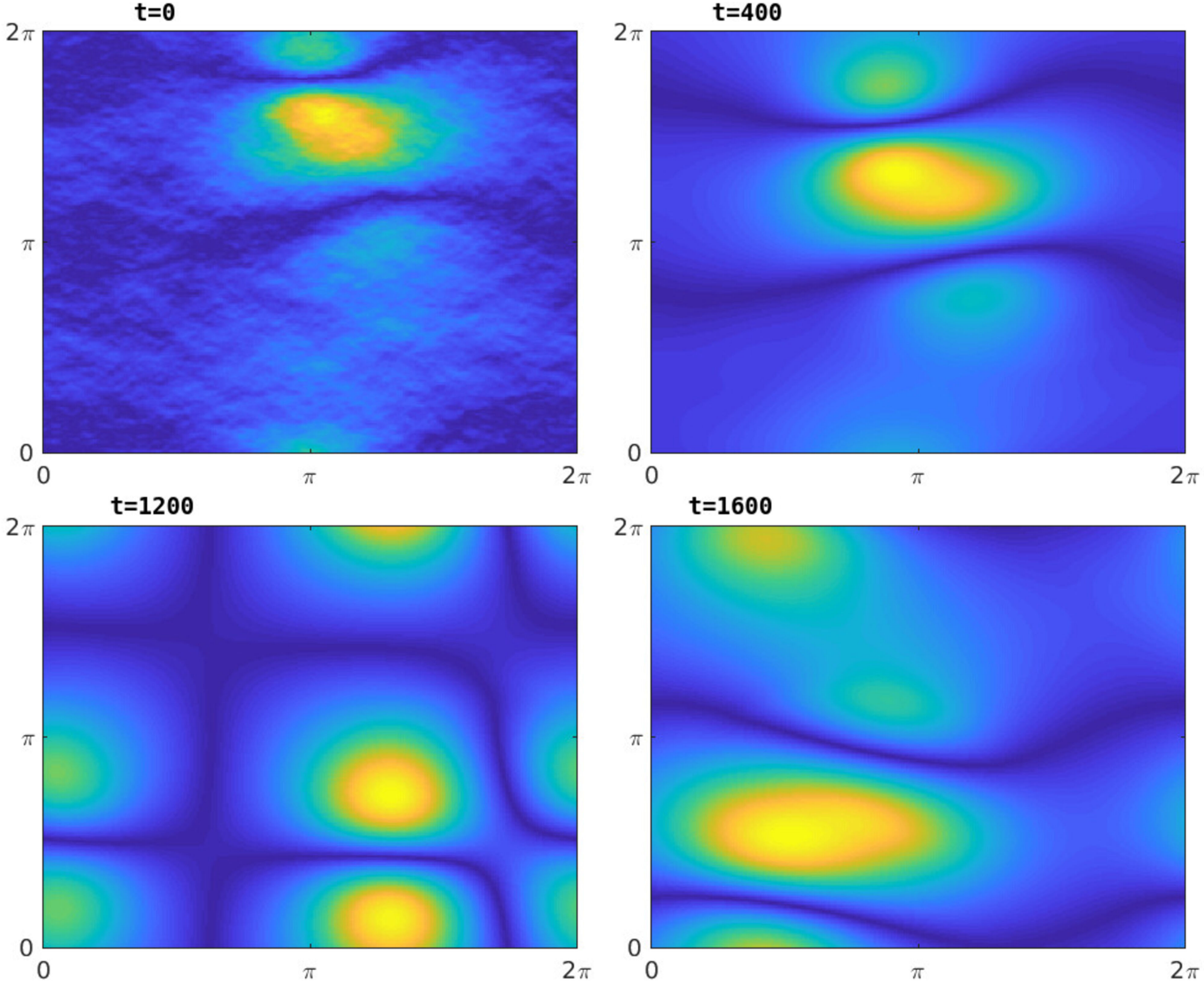
t=0
t=400
t=1200
t=1600
2π
π
0
0
π
2π

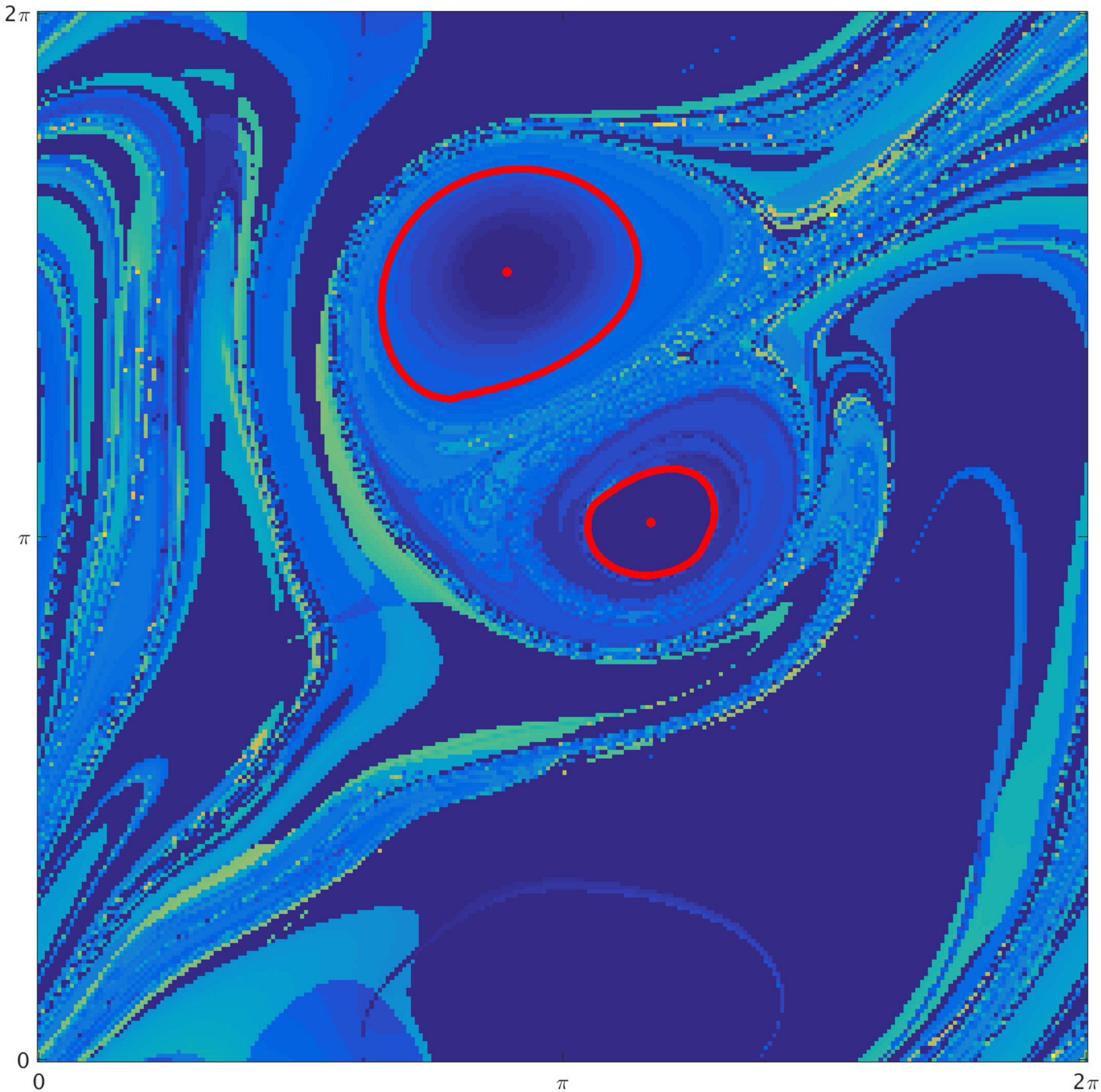
2π
π
0
0
π
2π

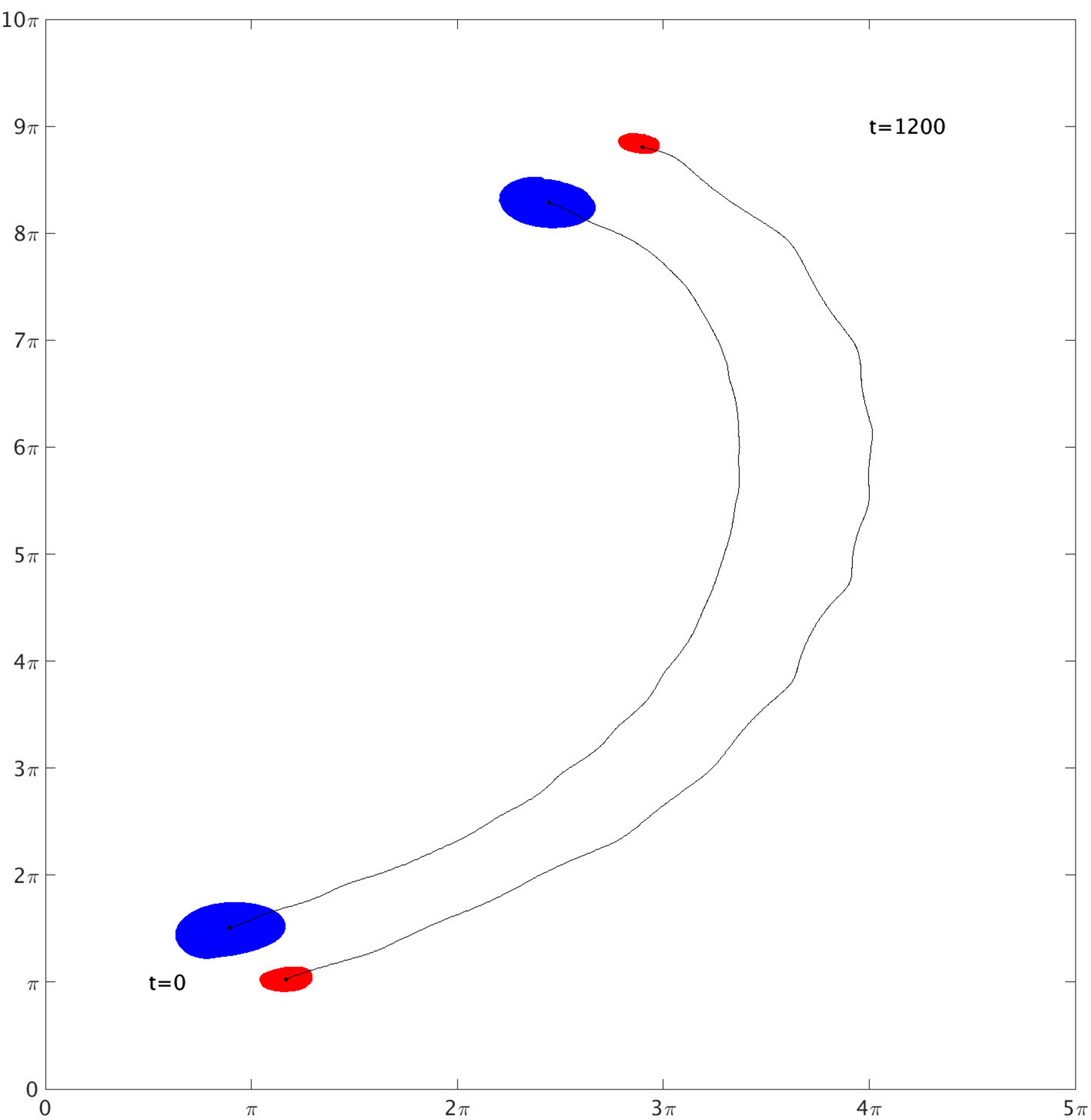
t=1200
t=0
10π
9π
8π
7π
6π
5π
4π
3π
2π
π
0
0
π
2π
3π
4π
5π

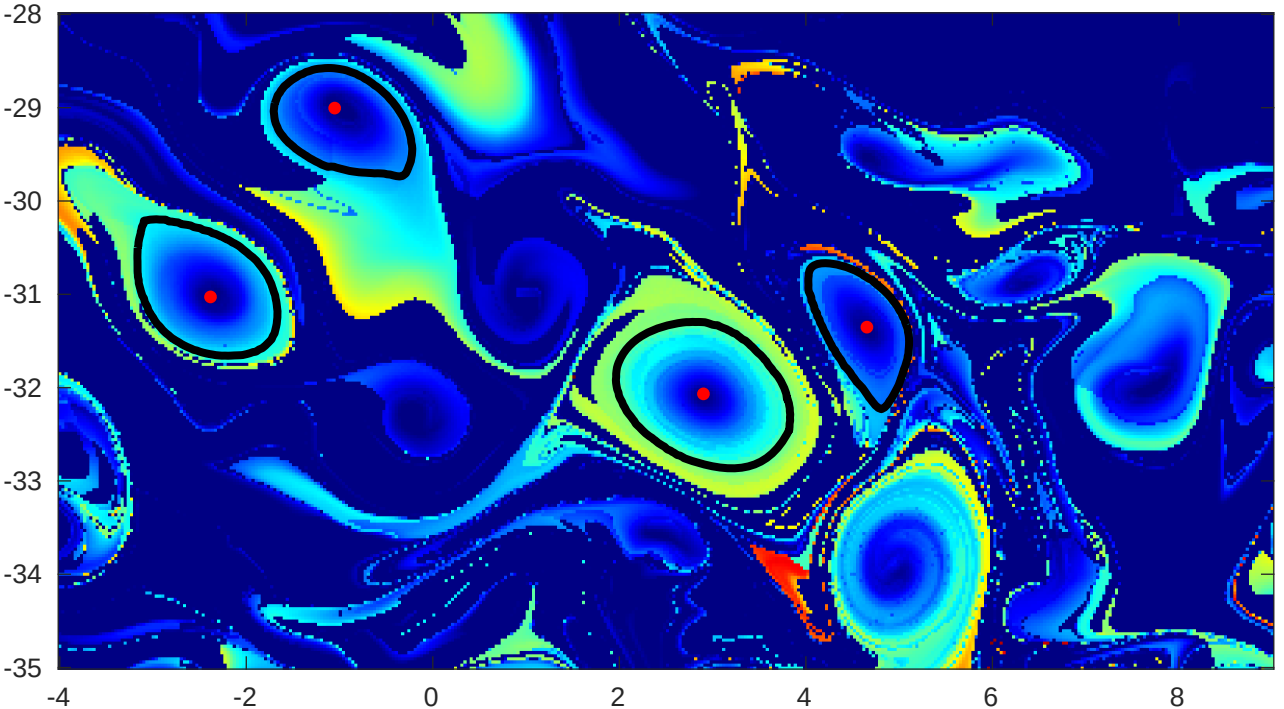
-28
-29
-30
-31
-32
-33
-34
-35
-4
-2
0
2
4
6
8

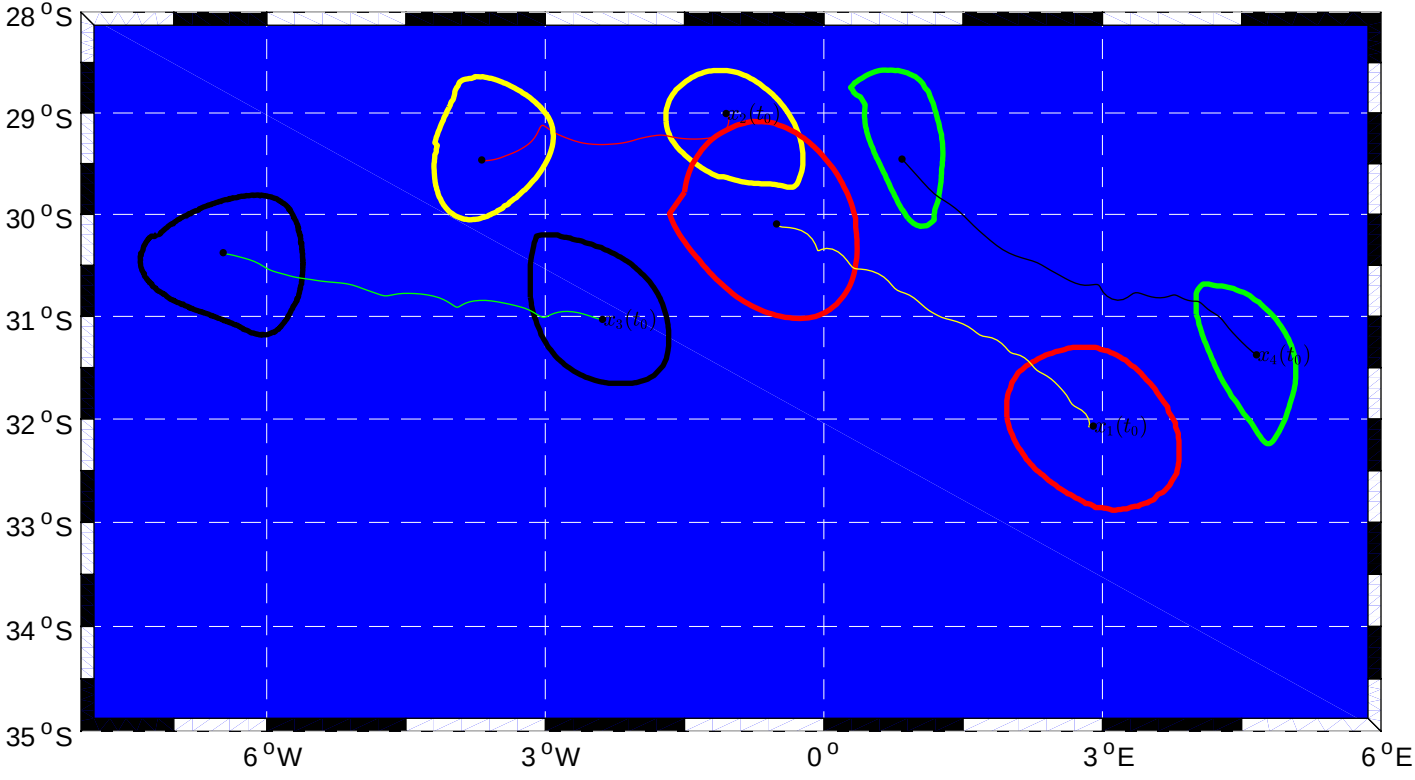
28 °S
29 °S
30 °S
31 °S
32 °S
33 °S
34 °S
35 °S
6 °W
3 °W
0 °
3 °E
6 °E
$x_2(t_0)$
$x_3(t_0)$
$x_4(t_0)$
$x_1(t_0)$

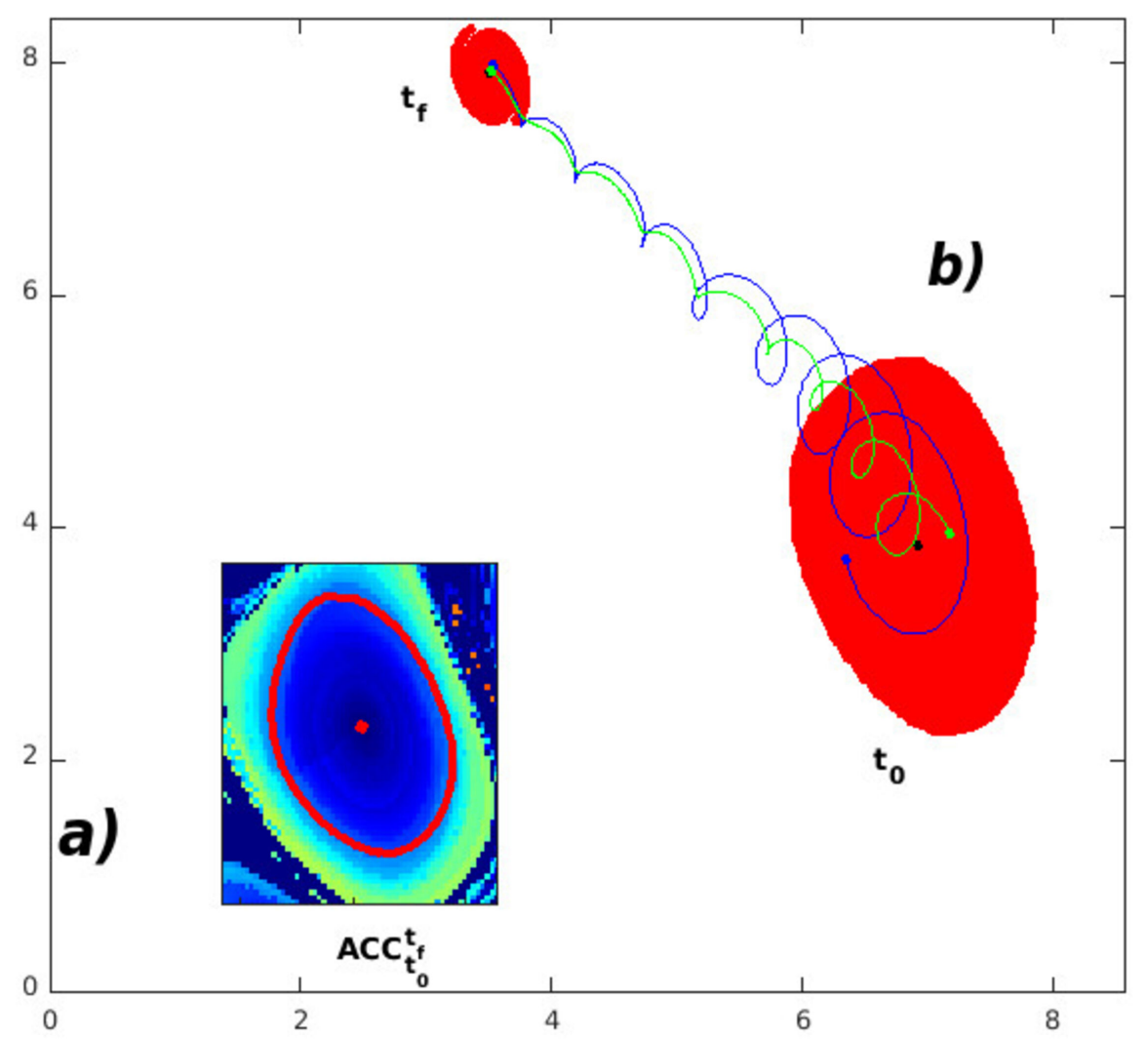
t_f
b)
t_0
a)
$ACC_{t_0}^{t_f}$
0
2
4
6
8